Optimization of Coaxial Magnetic Gear Design and Magnet Material Grade at Different Temperatures and Gear Ratios

Matthew C. Gardner, *Member, IEEE*, Bryton Praslicka, *Student Member, IEEE*, Matthew Johnson, *Member, IEEE*, and Hamid A. Toliyat, *Fellow, IEEE*

***Abstract*--Magnetic gears, like mechanical gears, transform power between different speeds and torques; however, magnetic gears' contactless nature provides inherent potential benefits over mechanical gears. A genetic algorithm was used to optimize magnetic gears at different temperatures across a range of gear ratios. Using different magnet material grades on the different rotors and for the tangentially and radially magnetized magnets can slightly increase the specific torque relative to designs with a single magnet material. The high pole count rotor requires a magnet material with higher coercivity than that of the low pole count rotor magnet material, especially for designs with a large gear ratio. While increasing the temperature produces an exponential decay in the achievable specific torque, with a compounding reduction of about 0.4% for each degree Celsius, the temperature does not significantly affect the optimal geometric parameters and primarily affects the optimal materials. The gear ratio significantly affects the optimal geometric parameters and can impact the optimal magnet materials. Additionally, the genetic algorithm was employed to characterize the impact of stack length using 3D finite element analysis. Designs with shorter stack lengths favored thinner magnets and higher pole counts and may be able to use magnet materials with lower coercivities.**

***Index Terms*--End effects, finite element analysis, genetic algorithm, magnetic gear, magnet grade, NdFeB, permanent magnet, SmCo, specific torque, temperature, torque density**

I. Introduction

In 2018, transportation accounted for the largest portion (28%) of total U.S. greenhouse gas emissions, and aircraft were the third largest contributor to transportation end-use emissions, constituting 9% of the sector [1]. NASA identified electric aircraft propulsion (EAP) as a key enabler to achieve the aggressive goals set for the efficiency, emissions, reliability, and noise standards of the next generation of fixed wing and vertical lift aircraft. These standards were set to meet the growing global concern for the environment [2] and demands of the short haul markets for last-mile delivery and air metros, which could become billion-dollar industries by 2030 according to separate market studies [3], [4]. The addition of a mechanical gearbox to an electric aircraft powertrain has been shown to reduce the powertrain system weight [5]. However, the operation and maintenance cost of any aircraft with a mechanical gearbox increases due to the increased maintenance needs [6]. Moreover, rotorcraft commercial adoption is hindered by excessive cabin noise (often exceeding 100 dB), caused primarily by structural vibrations originating from the main rotor gearbox meshing [7].

Magnetic gearboxes convert energy between low-speed, high-torque rotation and high-speed, low-torque rotation. Like mechanical gearboxes, magnetic gearboxes allow a relatively small, high-speed electric machine to connect to a low-speed high-torque system. Magnetic gearboxes distinguish themselves from mechanical gearboxes by transferring power using modulated magnetic fields rather than the meshing of gear teeth. The contactless operation of magnetic gearboxes provides a plethora of potential benefits, such as improved reliability, reduced maintenance, reduced acoustic noise, and physical isolation between shafts. Thus, magnetic gearboxes have generated significant interest over the past twenty years [8]-[10], leading NASA to create a multiyear project to study magnetic gearing technology for electric aviation propulsion [6], [11], [12]. In addition to electric aviation propulsion, magnetic gears have been proposed for numerous other applications, including wind [13]-[15] and wave [16] energy, traction [17], [18], and hybrid electric vehicle power split devices [19].

Fig. 1 shows a comparison of specific torques (torque densities) for select magnetic gear prototypes [6], [11]-[13] [17], [20]-[22] and select rotorcraft and fixed wing aircraft mechanical transmissions [11], [23]. The magnetic gear prototype specific torques are shown based on both active mass (the mass of the magnetically active components, such as permanent magnets (PMs) and electric steel) and total mass (the active mass plus the mass of magnetically inactive components, such as support structures). The black trendline in Fig. 1 is a curve fit of the mechanical transmission specific torques and it

This work was supported in part by the U.S. Army CCDC Army Research Laboratory.

M. C. Gardner was with the Advanced Electric Machines and Power Electronics Lab at Texas A&M University, College Station, TX 77843 USA. He is now with the University of Texas at Dallas, Dallas, TX 75080 USA (e-mail: Matthew.Gardner@utdallas.edu).

B. Praslicka is with the Advanced Electric Machines and Power Electronics Lab at Texas A&M University, College Station, TX 77843 USA (e-mail: bryton.praslicka@tamu.edu).

M. Johnson is with the U.S. Army CCDC Army Research Laboratory, College Station, TX 77843 USA (e-mail: matthew.c.johnson186.civ@mail.mil).

H. A. Toliyat is with the Advanced Electric Machines and Power Electronics Lab at Texas A&M University, College Station, TX 77843 USA (e-mail: toliyat@tamu.edu).

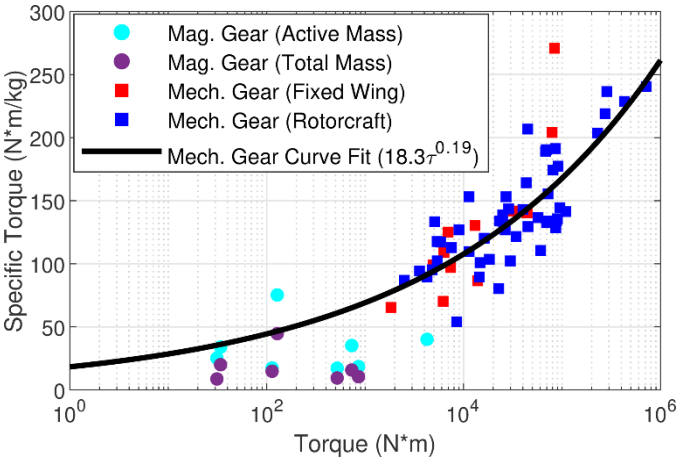

Fig. 1. Comparison of specific torques for select magnetic gear prototypes (based on both active mass and total mass) and select rotorcraft and fixed wing aircraft mechanical transmissions. The black line indicates a curve fit of both the rotorcraft and fixed wing aircraft mechanical transmission specific torques.

indicates that a transmission's specific torque tends to increase with its torque rating. A comparison of the different data sets shows that, to date, the magnetic gear prototypes produced generally have lower specific torques and lower torque ratings. While it is anticipated that the magnetic gear specific torques will also increase with the torque rating, most of the magnetic gear data points fall below the mechanical transmission trendline. This disparity is partially a result of the fact that the magnetic gear data points are based on laboratory prototypes, which are often conservative or not fully optimized, and the mechanical transmissions correspond to mature technology readiness level (TRL) 9 aircraft transmissions [11]. However, this comparison also indicates the importance of maximizing a magnetic gear's specific torque in order to make the technology competitive with mechanical transmissions, especially for applications in which weight is critical, such as aviation.

This study focuses on the radial flux coaxial magnetic gear topology with Halbach arrays, which has demonstrated high performance for the primary EAP powertrain design objectives [12] of efficiency [22], [24] and specific torque [6], [11], [12]. As depicted in Fig. 2, coaxial magnetic gears have three concentric rotors: Rotor 1, which has P_1 PM pole pairs, Rotor 2, which consists of Q_2 ferromagnetic modulators interspersed with nonmagnetic material, and Rotor 3, which has P_3 PM pole pairs. For optimal operation, the counts are related by

$$Q_2 = P_1 + P_3. \tag{1}$$

In this case, the speeds of Rotors 1, 2, and 3 (ω_1, ω_2, and ω_3, respectively) are related by

$$\omega_1 P_1 - \omega_2 Q_2 + \omega_3 P_3 = 0. \tag{2}$$

The largest gear ratio (G) between any two rotors is achieved by fixing Rotor 3, which results in

$$G|_{\omega_3=0} = \frac{\omega_1}{\omega_2} = \frac{Q_2}{P_1}. \tag{3}$$

As in Fig. 2, only two PM pieces per pole are used on Rotors 1 and 3 in this study because increasing the number of PM pieces

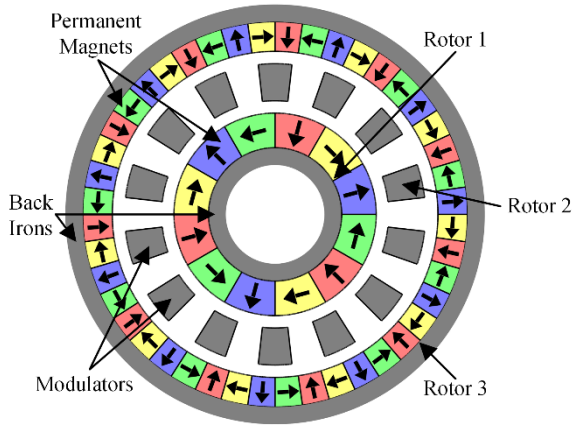

Fig. 2. Magnetically active components of a radial flux coaxial magnetic gear with Halbach arrays.

further yields diminishing returns for specific torque [25] while increasing complexity.

While there are numerous comparisons of magnet materials for the radial flux coaxial magnetic gear with surface permanent magnets (SPM), [26]-[30], there are no known studies that thoroughly analyze the optimal Neodymium Iron Boron (NdFeB) magnet grade selection for any magnetic gear topology. It was not until 2018 that researchers published about using different grades of NdFeB for Rotor 1 and Rotor 3 of the magnetic gear [12], [31], and NASA was the first to write an optimization algorithm to select a grade for a single operating temperature while considering demagnetization [12]. None of these studies thoroughly evaluate the impact of temperature on the performance of magnetic gears. Different grades of NdFeB magnets have been studied for SPM generators [32], and IPM motors [33], [34], at different operating temperatures, but no known study exists for aerospace specific applications. NdFeB magnets are of particular interest for aerospace applications, as NASA predicts motors used in commercial aircraft driven by electric propulsion will use NdFeB permanent magnet technology unless operating temperatures require Samarium Cobalt (SmCo) magnets [35]. Additionally, as [30] observes, SPM magnetic gears with NdFeB magnets can generally achieve higher specific torques and lower costs than gears with ferrite magnets. NASA only considered NdFeB for their magnetic gear prototypes [6], [11], [12], assuming an operating temperature of 100°C [12]. The operating temperatures of existing vertical takeoff and landing (VTOL) aircraft transmissions, such as the tail rotor of the Bell 206B (maximum transmission oil continuous operating temperature rated at 110°C) [36] or the main gear box of the UH-60A Black Hawk helicopter (measured 132°C maximum) [37] do not exceed 150°C. Based on [12], in which a magnetic gear prototype is designed for a future electric VTOL (eVTOL) concept vehicle, it is reasonable to assume that operating temperatures for such vehicles will be below 150°C.

This paper is the first to thoroughly examine the optimal grade of NdFeB magnet for SPM radial flux coaxial magnetic gears with Halbach arrays for a variety of operating temperatures. This paper also evaluates using different grades of NdFeB for the radial and tangential components of the Halbach array on a particular rotor.

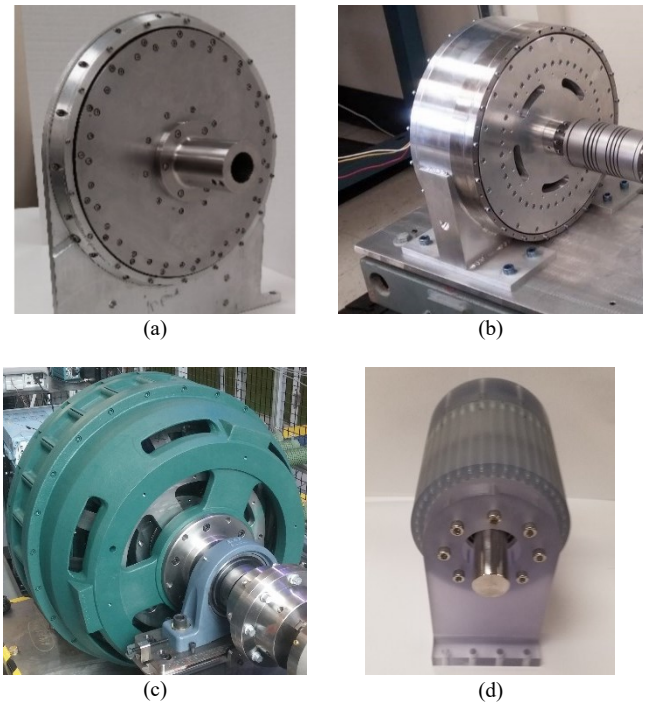

(a) (b) (c) (d)

Fig. 3. Previous (a) axial flux coaxial magnetic gear [38], (b) axial flux coaxial magnetically geared machine [39], (c) radial flux coaxial magnetically geared machine [16], and (d) radial flux coaxial magnetic gear with Halbach arrays [22] prototypes tested by the authors.

TABLE I
Comparison between Authors' Previous FEA and Prototype Measurements

Reference	[38]	[39]	[16]	[22]
Year Published	2014	2017	2018	2019
FEA low-speed rotor slip torque (N·m)	38.0	42.1	3905	30.4
Measured low-speed rotor slip torque (N·m)	40.2	42.2	3870	31.2
Difference between FEA and measurement	-5.5%	-0.2%	0.9%	-2.6%

This paper uses finite element analysis (FEA) and does not present new hardware experimental results. Whereas some past studies by various groups have previously yielded significant discrepancies between FEA and prototype results, often larger than 10%, the authors have demonstrated that their FEA models accurately and consistently predict the slip torques of magnetic gear and magnetically geared machine prototypes [16], [22], [38], [39], including a prototype with Halbach arrays [22]. The agreements between the authors' previous FEA predictions and prototype measurements are summarized in Fig. 3 and Table I. It would be impractical to fabricate prototypes with many different magnet grade combinations and test each of them with different controlled magnet temperatures. However, experimentally validated models using the B-H curves from the magnet supplier can address extremely practical temperature and magnet grade considerations.

II. Design Study Methodology

As in previous studies of electric machines [40] and magnetic gears [41]-[43], the GOSET genetic algorithm (GA) [44] was used to perform 36 multi-objective optimizations. These optimizations were performed at 6 different PM temperatures, 20 °C, 60 °C, 80 °C, 100 °C, 120 °C, and 150 °C, based on the available PM B-H curves [45], [46]. Additionally, 3 different PM material constraint scenarios were considered: all of the PMs had to be the same material, all of the PMs on each rotor had to be the same material but Rotors 1 and 3 could have different materials, or the tangentially and radially magnetized PMs could use different materials on each rotor. Finally, the optimizations were performed with and without a demagnetization constraint. The constraint imposed was that less than 1% of the PM volume on each rotor should be below the knee points shown in Table II when the design is at the slip torque point. This constraint is a simplification that does not reflect the full impacts of different loads but is intended to indicate roughly whether a design will be susceptible to significant irreversible demagnetization or not. The entries in Table II with N/A indicate temperatures where the B-H curve was not available for that material. The materials in Table II represent the strongest magnet grades available for each NdFeB temperature suffix and a strong grade of SmCo. As the primary focus of this optimization is on mass, rather than cost, weaker grades of NdFeB or SmCo were not considered. The modulators and back irons material were Hiperco 50, which was assumed to have negligible variation in its B-H curve within the range of considered temperatures [47].

For each optimization, the genetic algorithm used 2D finite element analysis (FEA) to optimize a population of 1000 designs over 200 generations with the objective of simultaneously maximizing both gear ratio and specific torque, which is the Rotor 2 slip torque divided by the total active mass. In addition to the different materials considered in Table II, Table III provides the other parameters swept and the ranges considered for each parameter.

TABLE II
Knee Points for Different PM Materials and Temperatures

	20 °C	**60 °C**	**80 °C**	**100 °C**	**120 °C**	**150 °C**
NdFeB N55	0.31 T	0.57 T	0.70 T	0.81 T	0.89 T	N/A
NdFeB N52M	0.05 T	0.40 T	0.52 T	0.68 T	0.77 T	0.90 T
NdFeB N50H	-0.30 T	0.08 T	0.25 T	0.44 T	0.55 T	0.72 T
NdFeB N48SH	-0.65 T	-0.19 T	0.01 T	0.20 T	0.33 T	0.54 T
NdFeB N45UH	-1.22 T	-0.71 T	-0.48 T	-0.26 T	-0.08 T	0.21 T
NdFeB N42EH	-1.80 T	-1.26 T	-1.01 T	-0.77 T	-0.55 T	-0.24 T
SmCo Recoma 35 E	-1.20 T	N/A	N/A	-0.73 T	N/A	-0.46 T

TABLE III
Genetic Algorithm Parameter Ranges

Parameter	**Description**	**Range**	**Units**
G_{Int}	Integer portion of the gear ratio	3-15	
P_1	Rotor 1 pole pairs	3-30	
R_{Out}	Gear active outer radius	100	mm
T_{BI1}	Rotor 1 back iron thickness	0-10	mm
T_{PM1}	Rotor 1 magnet thickness	3-20	mm
T_{AG1}	Inner air gap thickness	0.5	mm
T_{Mods}	Modulator thickness	5-15	mm
T_{AG2}	Outer air gap thickness	0.5	mm
k_{PM}	Magnet thickness ratio	0.05-1	
T_{BI3}	Rotor 3 back iron thickness	0-10	mm
α_{Mods}	Modulator fill factor	0.35-0.65	
α_{Rad1}	Rotor 1 radial PM fill factor	0.1-0.9	
α_{Rad3}	Rotor 3 radial PM fill factor	0.1-0.9	

A few other parameters are defined in terms of the parameters in Table III. First, the number of Rotor 3 pole pairs (P_3) is given by

$$P_3 = \begin{cases} (G_{Int} - 1)P_1 + 1 & \text{for } G_{Int}P_1 \text{ odd} \\ (G_{Int} - 1)P_1 + 2 & \text{for } G_{Int}P_1 \text{ even.} \end{cases} \quad (4)$$

This avoids integer gear ratios, which are prone to large torque ripples [12], [15], [31], and designs without any symmetry, which can experience significant unbalanced magnetic forces on the rotors [16], [48]. Second, the Rotor 3 PM thickness (T_{PM3}) is defined by

$$T_{PM3} = k_{PM}T_{PM1}, \quad (5)$$

as in [16], [43]. Additionally, the net PM fill factors on Rotors 1 and 3 are set to unity, as in Fig. 2, so that the Rotor 1 and Rotor 3 tangentially magnetized PM fill factors (α_{Tan1} and α_{Tan3}) are given by

$$\alpha_{Tan1} = 1 - \alpha_{Rad1} \quad (6)$$

$$\alpha_{Tan3} = 1 - \alpha_{Rad3}. \quad (7)$$

III. Results

Figs. 4 and 5 show the Pareto optimal fronts maximizing specific torque and gear ratio for the different optimizations. The specific torques shown in Fig. 5 are significantly higher than those shown for past magnetic gear prototypes in Fig. 2. This difference is due to a combination of factors, including this study's use of more aggressive, but achievable 0.5 mm air gaps, consideration of aggressively thin modulators and light weight air core designs with no back irons, thorough optimizations, and neglection of structural mass and 3D end effects, which can appreciably reduce a design's torque rating depending on its form factor. As shown in previous studies [43], Fig. 5 illustrates a significant reduction in specific torque as the gear ratio increases. Additionally, increasing the temperature decreases the achievable specific torque, which may limit the suitability of magnetic gears for high temperature applications. Fig. 5 also shows that the percentage reduction in specific torque as temperature increases is quite consistent across the range of gear ratios, with an exponential decay of about 0.4% compounding for each degree Celsius increase in temperature throughout the evaluated range of gear ratios and temperatures, assuming the optimal PM materials are used in each case. Additionally, Fig. 5 indicates that using different materials for the different sets of PMs can increase specific torque by a few percent, especially for higher gear ratio designs. Finally, Fig. 5 shows that considering demagnetization does impact the optimal designs produced by the GA.

While the temperature significantly affects the achievable specific torques, it did not affect the optimal values of most design parameters in this study. For all the optimizations, the optimal designs had no back irons ($T_{BI1} = T_{BI3} = 0$ mm), modulators with the minimum radial thickness ($T_{Mods} = 5$ mm), and approximately 50% fill factors for the Rotors 1 and 3 radially and tangentially magnetized PMs ($\alpha_{Rad1} \approx \alpha_{Rad3} \approx 0.5$). This is consistent with the magnetic gear designs closest to the power model regression in Fig. 1, which had no back iron (air cores) and used thin modulators [6], [11], [22]. Air core designs are made possible by Halbach magnet arrangements and can be implemented with lightweight polymeric composites for structural material. Thin modulators can be supported with

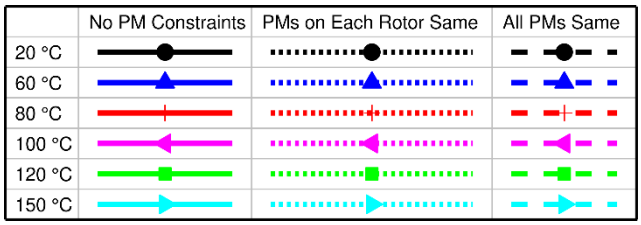

Fig. 4. Legend for Figs. 5-9.

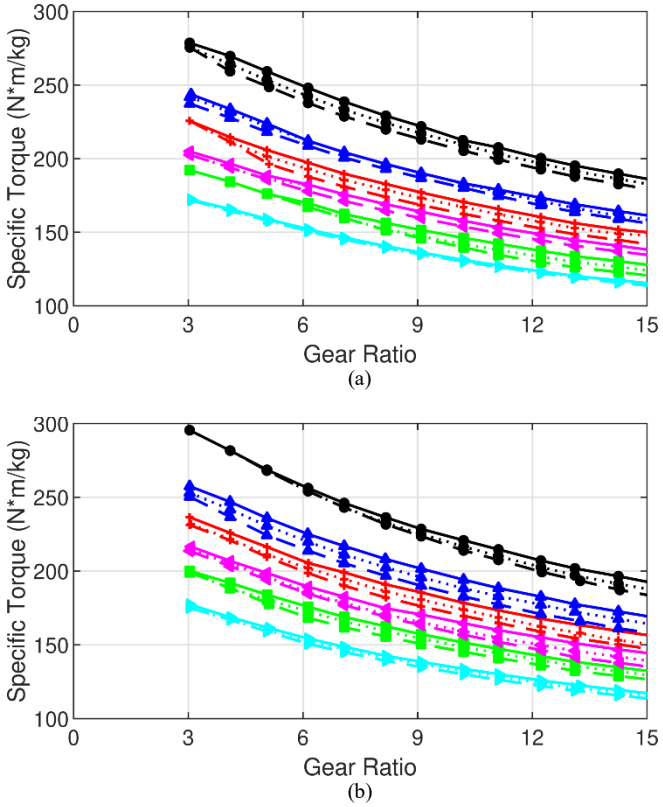

Fig. 5. Maximum specific torque achievable across a range of gear ratios resulting from the GA optimizations at different temperatures, with different PM material constraints, and (a) with or (b) without a demagnetization constraint.

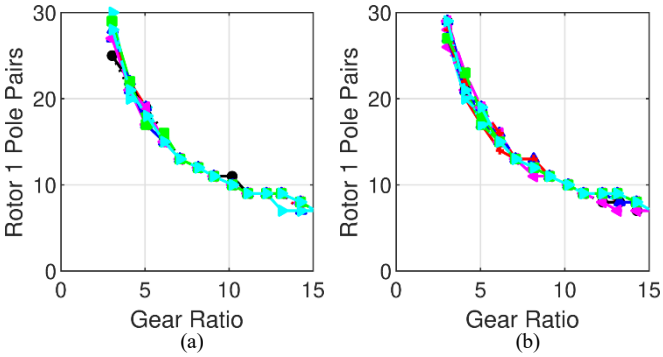

Fig. 6. Optimal Rotor 1 pole pair counts for maximizing the specific torque achievable across a range of gear ratios resulting from the GA optimizations at different temperatures, with different PM material constraints, and (a) with or (b) without a demagnetization constraint.

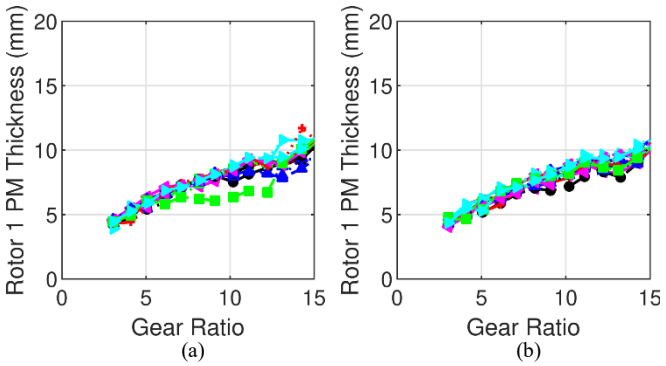

Fig. 7. Optimal Rotor 1 PM thicknesses for maximizing the specific torque achievable across a range of gear ratios resulting from the GA optimizations at different temperatures, with different PM material constraints, and (a) with or (b) without a demagnetization constraint.

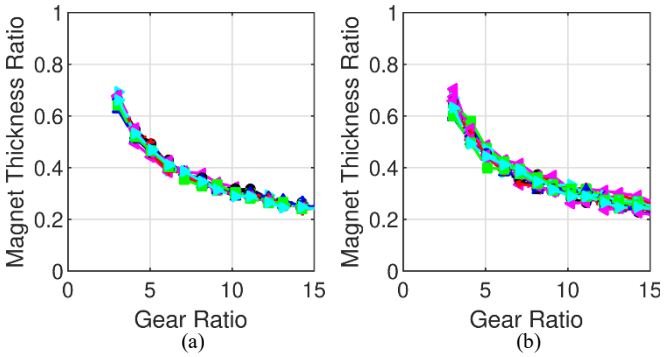

Fig. 8. Optimal PM thickness ratios for maximizing GTD achievable across a range of gear ratios resulting from the GA optimizations at different temperatures, with different PM material constraints, and (a) with or (b) without a demagnetization constraint.

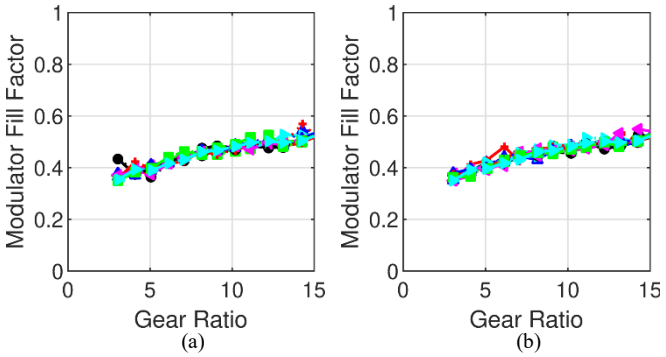

Fig. 9. Optimal modulator fill factors for maximizing the specific torque achievable across a range of gear ratios resulting from the GA optimizations at different temperatures, with different PM material constraints, and (a) with or (b) without a demagnetization constraint.

material such as glass-filled Nylon [22] or carbon fiber [11]. While the aforementioned design settings were consistent, the optimal values of other parameters changed with the gear ratio, as indicated in Figs. 6-9. The points illustrated in Figs. 6-9 corresponds to the points in Fig. 5.

While the limited precision of FEA and the finite number of cases evaluated do result in some noise in the graphs, Figs. 6-9 show that the optimal geometric design parameter values depend primarily on gear ratio rather than temperature or the material or demagnetization constraints imposed in the study. As indicated in previous studies [30], [43], increasing the gear ratio decreases the optimal Rotor 1 pole pair count, which is correlated with an increase in the optimal Rotor 1 PM thickness. Additionally, as the gear ratio increases, the growing difference between the Rotor 1 and Rotor 3 pole pair counts leads to an increasing difference in the optimal Rotor 1 and Rotor 3 PM thicknesses. Finally, increasing the gear ratio also increases the optimal modulator fill factor, which partially compensates for the reduced modulator tangential widths resulting from the higher modulator counts associated with larger gear ratios.

As expected, changing the temperature does significantly change the optimal PM materials, which are listed in Tables IV-VI for designs with a few different gear ratios. Table IV shows the results for studies in which there was no constraint on PM material uniformity, and it shows that the optimal designs may use different material grades for the radially (r) and tangentially (θ) magnetized PMs. Additionally, Tables IV-V reveal that the Rotor 3 PMs generally require materials with higher coercivities than the Rotor 1 PMs; as the gear ratio increases, this trend becomes more significant. This trend is tied to the longer pole arcs of Rotor 1 (Fig. 6) and the decreasing PM thickness ratio (Fig. 8). Additionally, while these tables show a significant difference in the optimal materials selected when constraining demagnetization, these trends are evident even for the cases where demagnetization was not constrained, due to the nonlinearity of the PM B-H curves.

Fig. 10 shows the variation in maximum specific torque of the $G_{Int} = 6$ designs with temperature for different PM materials, when the PM material is constrained to be the same throughout

TABLE IV
Optimal PM Materials for the Different Rotors and Magnetization Directions with No PM Material Constraint

		Demagnetization Constraint			Demagnetization Allowed		
		$G_{Int} = 3$	$G_{Int} = 7$	$G_{Int} = 15$	$G_{Int} = 3$	$G_{Int} = 7$	$G_{Int} = 15$
20 °C	Rotor 1r	N52M	N52M	N52M	N55	N55	N55
	Rotor 1θ	N52M	N55	N55	N55	N55	N55
	Rotor 3r	N52M	N52M	N52M	N55	N55	N55
	Rotor 3θ	N50H	N50H	N48SH	N55	N52M	N50H
60 °C	Rotor 1r	N50H	N50H	N50H	N55	N55	N55
	Rotor 1θ	N50H	N50H	N52M	N55	N55	N55
	Rotor 3r	N50H	N48SH	N50H	N55	N55	N55
	Rotor 3θ	N48SH	N48SH	N45UH	N50H	N48SH	N48SH
80 °C	Rotor 1r	N48SH	N50H	N50H	N55	N52M	N50H
	Rotor 1θ	N48SH	N48SH	N50H	N50H	N55	N55
	Rotor 3r	N48SH	N48SH	N48SH	N55	N55	N55
	Rotor 3θ	N48SH	N45UH	N45UH	N50H	N48SH	N45UH
100 °C	Rotor 1r	N45UH	N48SH	N48SH	N50H	N50H	N50H
	Rotor 1θ	N48SH	N48SH	N48SH	N50H	N50H	N55
	Rotor 3r	N45UH	N45UH	N45UH	N55	N55	N55
	Rotor 3θ	N45UH	N45UH	N45UH	N48SH	N45UH	N45UH
120 °C	Rotor 1r	N45UH	N45UH	N45UH	N50H	N48SH	N48SH
	Rotor 1θ	N45UH	N48SH	N48SH	N48SH	N50H	N50H
	Rotor 3r	N45UH	N45UH	N45UH	N50H	N50H	N50H
	Rotor 3θ	N45UH	N42EH	N42EH	N45UH	N45UH	N45UH
150 °C	Rotor 1r	35E	35E	N45UH	N48SH	N45UH	N45UH
	Rotor 1θ	N45UH	N45UH	N45UH	N45UH	N48SH	N48SH
	Rotor 3r	35E	35E	35E	N48SH	N48SH	N48SH
	Rotor 3θ	35E	N42EH	N42EH	N45UH	N42EH	N42EH

TABLE V
Optimal PM Materials for the Different Rotors with the PM Material Constrained to be the Same for Radially and Tangentially Magnetized PMs on Each Rotor

		Demagnetization Constraint			Demagnetization Allowed		
		G_{Int} = 3	G_{Int} = 7	G_{Int} = 15	G_{Int} = 3	G_{Int} = 7	G_{Int} = 15
20 °C	Rotor 1	N52M	N52M	N52M	N55	N55	N55
	Rotor 3	N52M	N50H	N50H	N55	N55	N50H
60 °C	Rotor 1	N50H	N50H	N50H	N55	N55	N55
	Rotor 3	N48SH	N48SH	N48SH	N52M	N50H	N48SH
80 °C	Rotor 1	N48SH	N48SH	N50H	N52M	N55	N55
	Rotor 3	N48SH	N45UH	N45UH	N50H	N48SH	N48SH
100 °C	Rotor 1	N45UH	N48SH	N48SH	N50H	N50H	N50H
	Rotor 3	N45UH	N45UH	N45UH	N48SH	N48SH	N45UH
120 °C	Rotor 1	N45UH	N45UH	N45UH	N48SH	N48SH	N48SH
	Rotor 3	N45UH	N45UH	N42EH	N48SH	N45UH	N45UH
150 °C	Rotor 1	35E	35E	N45UH	N45UH	N48SH	N45UH
	Rotor 3	35E	35E	35E	N45UH	35E	35E

TABLE VI
Optimal PM Materials with the PM Material Constrained to be the Same Throughout Each Design

	Demagnetization Constraint			Demagnetization Allowed		
	G_{Int} = 3	G_{Int} = 7	G_{Int} = 15	G_{Int} = 3	G_{Int} = 7	G_{Int} = 15
20 °C	N52M	N50H	N50H	N55	N55	N55
60 °C	N48SH	N48SH	N48SH	N55	N50H	N50H
80 °C	N48SH	N45UH	N45UH	N50H	N50H	N48SH
100 °C	N45UH	N45UH	N45UH	N50H	N48SH	N48SH
120 °C	N45UH	N45UH	N42EH	N48SH	N45UH	N45UH
150 °C	35E	35E	35E	N45UH	35E	35E

a design and the demagnetization constraint is applied. Fig. 10 demonstrates that the specific torques of designs using PM materials with higher nominal maximum energy products and lower temperature tolerances decrease more rapidly with temperature than those of designs using PM materials with lower nominal maximum energy products and higher temperature tolerances. The decrease in specific torque with temperature is partially due to the decay of each material's B-H curve with temperature; however, in some instances, it is also a result of evolutions in the geometry of these designs to configurations which are less vulnerable to demagnetization (to help counteract the reduced coercivity of the materials at higher temperatures), but less conducive to high specific torque. This is especially true for the designs based on high maximum energy product materials as the temperature begins to increase, such as the NdFeB N50H design at 60 °C and the NdFeB N48SH design at 80 °C. Note that the designs which do not exhibit the highest specific torque for a given temperature may also be somewhat artificially low due to not being fully optimized as a result of the nature of the GA.

Another important consideration is whether designing for a higher temperature will result in significantly reduced performance at a lower temperature. Fig. 11 shows the performance of the Fig. 5(a) G_{Int} = 6 designs with the maximum specific torques at temperatures equal to or lower than the nominal design temperature. (Operating above the nominal

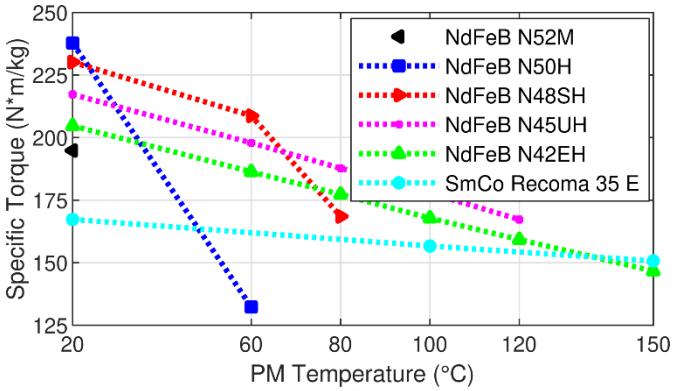

Fig. 10. Variation in specific torque with temperature of the G_{Int} = 6 designs optimized using different PM materials, when the PM material is constrained to be the same throughout a design and the demagnetization constraint is applied.

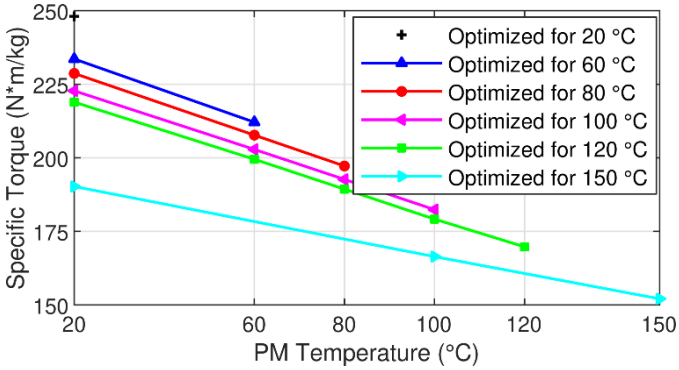

Fig. 11. Variation in specific torque with temperature of the G_{Int} = 6 designs optimized for different temperatures with no PM material constraints and with a demagnetization constraint.

design temperature would result in potential demagnetization.) Fig. 11 shows that designing a gear for too high a temperature does result in reduced specific torque at the actual operating temperature; this is especially significant if the temperature used for the optimization is high enough that SmCo magnets are optimal, as is the case at 150 °C.

IV. Impacts of End Effects

Previous studies have shown that end effects can significantly impact the torque [49] and optimal design parameters [42] for magnetic gears, especially for designs with short stack lengths. Therefore, the GA was also used with 3D FEA to characterize the optimal front for maximizing specific torque and minimizing stack length. Because 3D FEA is significantly slower than 2D FEA, the design space was narrowed to designs with G_{Int} = 7 at 100 °C. Additionally, based on the 2D FEA results, the range for P_1 was constrained between 8 and 20 inclusive, which eliminated the very high pole count simulations, which are especially slow. For this optimization, the same demagnetization constraint was applied, and the materials of the Rotors 1 and 3 radially and tangentially magnetized PMs were allowed to vary independently.

Fig. 12 illustrates how the achievable specific torque and some of the optimal design parameters vary with stack length based on 3D FEA simulations. Table VII compares the optimal PM materials based on 2D FEA and based on 3D FEA for three

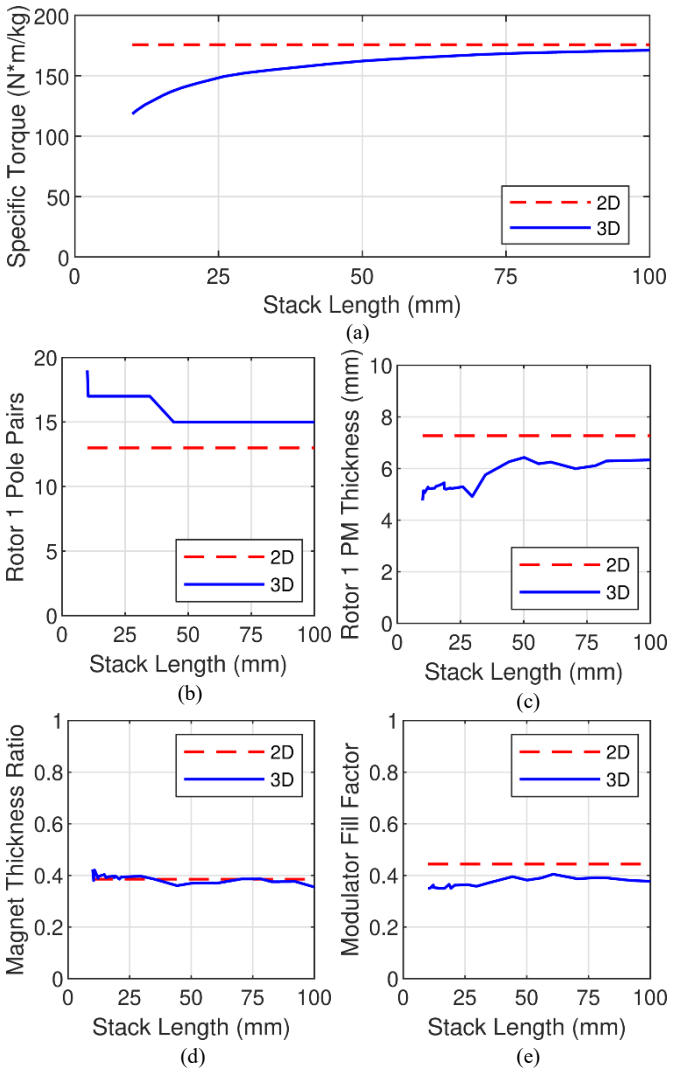

Fig. 12. Variation of (a) maximum achievable specific torque and the corresponding optimal (b) Rotor 1 pole pair counts, (c) Rotor 1 PM thicknesses, (d) PM thickness ratios, and (e) modulator fill factors at different stack lengths based on 2D and 3D FEA with the radially and tangentially magnetized PM materials on each rotor allowed to vary independently subject to a demagnetization constraint.

TABLE VII
2D FEA and 3D FEA Optimal PM Materials Comparison

	2D FEA	3D FEA		
Stack Length	**N/A**	**10 mm**	**35 mm**	**100 mm**
Rotor 1r	N48SH	N48SH	N48SH	N48SH
Rotor 1θ	N48SH	N50H	N48SH	N48SH
Rotor 3r	N45UH	N48SH	N48SH	N48SH
Rotor 3θ	N45UH	N45UH	N45UH	N45UH

different stack lengths. As in previous papers, the magnetic gear end effects produce a significant reduction in specific torque when 3D FEA is employed, especially for designs with relatively short stack lengths [42], [49]. Gears with short stack lengths favor thinner PMs and higher pole counts than designs with larger stack lengths. Additionally, the optimal modulator fill factor is reduced due to end effects because the modulators provide a relatively low reluctance path for flux to escape axially [49]. Furthermore, the leakage flux and axially escaping flux reduce the amount of demagnetization in the 3D simulations; this potentially results in optimal PM materials with lower coercivities than those of the optimal PM materials resulting from the 2D optimization, as shown in Table VII.

V. Conclusion

Temperature and material selection are critical aspects to consider in magnetic gear design. To investigate trends related to these phenomena, a GA using 2D FEA found the Pareto optimal fronts for maximizing specific torque and gear ratio at different temperatures and under different constraints. Fig. 13 illustrates the impacts of temperature and gear ratio on the achievable specific torque (neglecting structural masses), assuming that the optimal magnet materials are used. A GA optimization using 3D FEA was also performed at one temperature and gear ratio to evaluate how end effects impacted the optimal magnet grades. Based on these simulation studies, this paper contributes the following results and conclusions to the body of literature:

- Figs. 5, 10, 11, and 13 quantify the impact of magnet temperature on achievable magnetic gear performance. Throughout the design space evaluated in this study, the achievable specific torque decayed exponentially as the temperature increased, with a compounding decrease of about 0.4% for each degree Celsius, assuming that each design used the optimal PM materials for that temperature. This trend is consistent over the range of gear ratios evaluated in this study.
- Fig. 10 quantifies the impact of using different magnet grades on achievable magnetic gear performance. Whereas selecting a grade with a higher coercivity than the optimal grade slightly reduces the specific torque, selecting a grade with a lower coercivity than the optimal grade incurs a more significant penalty as the geometry must be adjusted to prevent demagnetization.
- Fig. 5 demonstrates the benefits of using different magnet grades on the different rotors and for the radially and tangentially magnetized pieces on each rotor. This can increase specific torque by a few percent, especially for designs with high gear ratios. As shown in Tables IV and V, designs with high gear ratios require higher coercivity magnets for Rotor 3 than for Rotor 1.

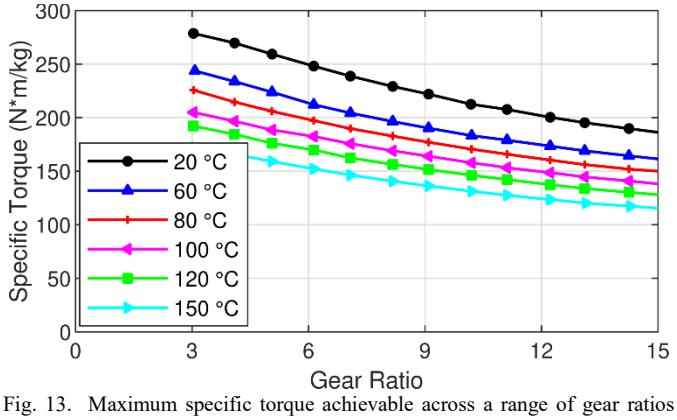

Fig. 13. Maximum specific torque achievable across a range of gear ratios resulting from the GA optimizations at different temperatures with a demagnetization constraint.

- Figs. 6 – 9 demonstrate that the temperature used during the optimization process primarily affects the optimal magnet grades and does not have a significant impact on the optimal geometric parameters.
- Tables IV – VI provide insight for selecting the appropriate magnet grades based on temperature and gear ratio. While the exactly optimal magnet grades may depend on the particular details of the design constraints, these tables provide a general starting point reference, and, in most cases, the optimal magnet grades for maximizing specific torque are expected to be within a grade or so of those listed in the tables.
- 3D simulation results summarized in Table VII demonstrate that end effects and their impacts on the optimal geometric parameters (Fig. 12) may result in a slightly lower coercivity PM material being optimal than would be indicated by 2D simulations, especially for designs with a short stack length.

VI. Acknowledgment

Portions of this research were conducted with the advanced computing resources provided by Texas A&M High Performance Research Computing. The authors would like to thank ANSYS for their support of the EMPE lab through the provision of FEA software.

VII. References

[1] Office of Transportation and Air Quality, "U.S. transportation sector greenhouse gas emissions," USA Environmental Protection Agency, Washington, DC, USA, Rep. no. EPA-420-F-20-037, Jun. 2020. [Online]. Available: https://www.epa.gov/sites/production/files/2020-07/documents/420f20037.pdf.

[2] NASA Aeronautics Research Mission Directorate, "Strategic implementation plan" Nat. Aeronaut. and Space Admin., Washington, DC, USA, Rep. NP-2017-01-2352-HQ, 2019. [Online]. Available: https://www.nasa.gov/sites/default/files/atoms/files/sip-2019-v7-web.pdf.

[3] H. Shahab, "Urban air mobility (UAM) market study," Crown Consulting Inc., Washington, DC, USA, Tech. Rep. no. HQ-E-DAA-TN70296, Jun. 2019.

[4] R. Goyal, "Urban air mobility (UAM) market study," Booz Allen Hamilton Inc., McLean, VA, USA, Tech. Rep. HQ-E-DAA-TN65181, Nov. 2018.

[5] A. D. Anderson *et al.*, "System weight comparison of electric machine topologies for electric aircraft propulsion," in *Proc. AIAA/IEEE Elect. Aircraft Technol. Symp.*, 2018, pp. 1-16.

[6] V. M. Asnani, J. J. Scheidler, and T. Tallerico, "Magnetic gearing research at NASA," in *Proc. of AHS Intl. 74th Annual Forum*, 2018, pp. 1-14.

[7] J. J. Scheidler, V. M. Asnani, "A review of noise and vibration control technologies for rotorcraft transmissions," NASA Glenn Res. Center, Cleveland, OH, USA, Tech. Rep. GRC-E-DAA-TN32233, Aug. 2016.

[8] K. Atallah and D. Howe, "A novel high-performance magnetic gear," *IEEE Trans. Magn.*, vol. 37, no. 4, pp. 2844–2846, Jul. 2001.

[9] P. O. Rasmussen, T. O. Anderson, F. T. Jorgensen, and O. Nielsen, "Development of a high performance magnetic gear," *IEEE Trans. Ind. Appl.*, vol. 41, no. 3, pp. 764–770, May/Jun. 2005.

[10] P. M. Tlali, R-J. Wang, and S. Gerber, "Magnetic gear technologies: A review," in *Proc. Int. Conf. Elect. Mach.*, 2014, pp. 544–550.

[11] J. J. Scheidler, V. M. Asnani and T. F. Tallerico, "NASA's magnetic gearing research for electrified aircraft propulsion," in *Proc. AIAA/IEEE Elect. Aircraft Technol. Symp.*, 2018, pp. 1-12.

[12] T. F. Tallerico, Z. A. Cameron and J. J. Scheidler, "Design of a magnetic gear for NASA's Vertical Lift Quadrotor Concept Vehicle," in *Proc. AIAA/IEEE Elect. Aircraft Technol. Symp.*, 2019, pp. 1-21.

[13] K. Li, S. Modaresahmadi, W. B. Williams, J. D. Wright, D. Som and J. Z. Bird, "Designing and experimentally testing a magnetic gearbox for a wind turbine demonstrator," *IEEE Trans. Ind. Appl.*, vol. 55, no. 4, pp. 3522-3533, Jul.-Aug. 2019.

[14] A. B. Kjaer, S. Korsgaard, S. S. Nielsen, L. Demsa and P. O. Rasmussen, "Design, fabrication, test, and benchmark of a magnetically geared permanent magnet generator for wind power generation," *IEEE Trans. Energy Conv.*, vol. 35, no. 1, pp. 24-32, Mar. 2020.

[15] N. W. Frank and H. A. Toliyat, "Gearing ratios of a magnetic gear for wind turbines," in *Proc. IEEE Int. Elect. Mach. Drives Conf.*, 2009, pp. 1224–1230.

[16] M. Johnson, M. C. Gardner, H. A. Toliyat, S. Englebretson, W. Ouyang, and C. Tschida, "Design, construction, and analysis of a large scale inner stator radial flux magnetically geared generator for wave energy conversion," *IEEE Trans. Ind. Appl.*, vol. 54, no. 4, pp. 3305–3314, Jul./Aug. 2018.

[17] P. O. Rasmussen, T. V. Frandsen, K. K. Jensen and K. Jessen, "Experimental evaluation of a motor-integrated permanent-magnet gear," *IEEE Trans. Ind. Appl.*, vol. 49, no. 2, pp. 850-859, March-April 2013.

[18] T. V. Frandsen *et al.*, "Motor integrated permanent magnet gear in a battery electrical vehicle," *IEEE Trans. Ind. Appl.*, vol. 51, no. 2, pp. 1516-1525, March-April 2015.

[19] P. Chmelicek, S. D. Calverley, R. S. Dragan and K. Atallah, "Dual rotor magnetically geared power split device for hybrid electric vehicles," *IEEE Trans. Ind. Appl.*, vol. 55, no. 2, pp. 1484-1494, March-April 2019.

[20] K. K. Uppalapati, W. B. Bomela, J. Z. Bird, M. D. Calvin and J. D. Wright, "Experimental evaluation of low-speed flux-focusing magnetic gearboxes," *IEEE Trans. Ind. Appl.*, vol. 50, no. 6, pp. 3637-3643, Nov.-Dec. 2014.

[21] K. K. Uppalapati, J. Z. Bird, J. Wright, J. Pitchard, M. Calvin and W. Williams, "A magnetic gearbox with an active region torque density of 239Nm/L," in *Proc. IEEE Energy Convers. Congr. and Expo.*, 2014, pp. 1422-1428.

[22] M. C. Gardner, M. Johnson and H. A. Toliyat, "Performance impacts of practical fabrication tradeoffs for a radial flux coaxial magnetic gear with Halbach arrays and air cores," in *Proc. IEEE Energy Convers. Congr. Expo.*, 2019, pp. 3129-3136.

[23] G. V. Brown *et al.*, "NASA Glenn Research Center Program in high power density motors for aeropropulsion," NASA Glenn Res. Center, Cleveland, OH, USA, Tech. Rep. TM—2005-213800, Dec. 2005.

[24] L. Jian, K. T. Chau, Y. Gong, J. Z. Jiang, C. Yu and W. Li, "Comparison of coaxial magnetic gears with different topologies," *IEEE Trans. Magn.*, vol. 45, no. 10, pp. 4526-4529, Oct. 2009.

[25] M. Johnson, M. C. Gardner and H. A. Toliyat, "Analysis of axial field magnetic gears with Halbach arrays," in *Proc. IEEE Int. Elect. Mach. Drives Conf.*, 2015, pp. 108-114.

[26] M. Chen, K. T. Chau, W. Li, and C. Liu, "Cost-effectiveness comparison of coaxial magnetic gears with different magnet materials," *IEEE Trans. Magn.*, vol. 50, no. 2, pp. 821–824, Feb. 2014.

[27] E. Park, S. Jung and Y. Kim, "Comparison of magnetic gear characteristics using different permanent magnet materials," *IEEE Trans. Appl. Supercond.*, vol. 30, no. 4, pp. 1-4, June 2020.

[28] M. Todorova, V. Mateev and I. Marinova, "Permanent magnets for a magnetic gear," in *Proc. Int. Symp. Elect. App. Technol.*, 2016, pp. 1-4.

[29] J. Shen, H. Li, H. Hao and M. Jin, "A coaxial magnetic gear with consequent-pole rotors," *IEEE Trans. Energy Conv.*, vol. 32, no. 1, pp. 267-275, Mar. 2017.

[30] M. Johnson, M. C. Gardner and H. A. Toliyat, "Design comparison of NdFeB and ferrite radial flux surface permanent magnet coaxial magnetic gears," *IEEE Trans. Ind. Appl.*, vol. 54, no. 2, pp. 1254-1263, Mar.-Apr. 2018.

[31] S. S. Nielsen, R. K. Holm, P. O. Rassmussen, "Conveyor system with a highly integrated permanent magnet gear and motor," in *Proc. IEEE Energy Convers. Congr. Expo.*, Sep. 2018, pp. 2359–2366.

[32] N. A. Bhuiyan and A. McDonald, "Optimization of offshore direct drive wind turbine generators with consideration of permanent magnet grade and temperature," *IEEE Trans. Energy Conver.*, vol. 34, no. 2, pp. 1105-1114, June 2019.

[33] S. Ruoho and A. Arkkio, "Mixed-grade pole design for permanent magnet synchronous machines," in *Proc. Int. Aegean Conf. Elect. Mach. Power Electron.*, 2007, pp. 452-457.

[34] A. Wang, H. Li and C. Liu, "On the material and temperature impacts of interior permanent magnet machine for electric vehicle applications," *IEEE Trans. Magn.*, vol. 44, no. 11, pp. 4329-4332, Nov. 2008.

[35] T. P. Dever *et al.*, "Assessment of technologies for noncryogenic hybrid electric propulsion," NASA Glenn Res. Center, Cleveland, OH, USA, Tech. Rep. TP—2015-216588, Jan. 2015.
[36] Bell Helicopter Textron Inc., "Bell Jet Ranger-III Rotorcraft Flight Manual – Model 206B," Fort Worth, TX, USA, Rep. BHT-206B3-FM-1, Revision 8, Oct. 2000.
[37] H. H. Coe, "Comparison of predicted and measured temperatures of UH-60A helicopter transmission," NASA Lewis Res. Center, Cleveland, OH, USA, Tech. Rep. NASA-TP-2911, Apr. 1989.
[38] M. Johnson, A. Shapoury, P. Boghrat, M. Post, and H. A. Toliyat, "Analysis and development of an axial flux magnetic gear," in *Proc. IEEE Energy Convers. Congr. and Expo*, 2014, pp. 5893-5900.
[39] M. Johnson, M. C. Gardner and H. A. Toliyat, "Design and Analysis of an Axial Flux Magnetically Geared Generator," *IEEE Trans. Ind. Appl.*, vol. 53, no. 1, pp. 97-105, Jan.-Feb. 2017.
[40] R. Lin, S. D. Sudhoff and V. C. do Nascimento, "A multi-physics design method for V-Shape interior permanent-magnet machines based on multi-objective optimization," *IEEE Trans. Energy Convers.*, vol. 35, no. 2, pp. 651-661, June 2020.
[41] J. M. Crider and S. D. Sudhoff, "An inner rotor flux-modulated permanent magnet synchronous machine for low-speed high-torque applications," *IEEE Trans. Energy Convers.*, vol. 30, no. 3, pp. 1247–1254, Sep. 2015.
[42] M. C. Gardner, B. E. Jack, M. Johnson, and H. A. Toliyat, "Comparison of surface mounted permanent magnet coaxial radial flux magnetic gears independently optimized for volume, cost, and mass," *IEEE Trans. Ind. Appl.*, vol. 54, no. 3, pp. 2237–2245, May/Jun. 2018
[43] M. C. Gardner, M. Johnson and H. A. Toliyat, "Analysis of high gear ratio capabilities for single-stage, series multistage, and compound differential coaxial magnetic gears," *IEEE Trans. Energy Convers.*, vol. 34, no. 2, pp. 665-672, June 2019.
[44] S. D. Sudhoff and Y. Lee, "Energy systems analysis consortium (ESAC) genetic optimization system engineering tool (GOSET) version manual," School Electr. Comput. Eng., Purdue Univ., West Lafayette, IN, USA, 2003.
[45] Arnold Magnetic Technologies Corp., Rochester, NY, USA, "Neodymium Iron Boron Magnet Catalog," Datasheet, Rev. 181031, 2019. [Online]. Available: https://www.arnoldmagnetics.com/wp-content/uploads/2019/06/Arnold-Neo-Catalog.pdf. Accessed Jul. 9, 2020.
[46] Arnold Magnetic Technologies Corp., Rochester, NY, USA, "Recoma 35E," Datasheet, 2017. [Online]. Available: https://www.arnold magnetics.com/wp-content/uploads/2017/10/Arnold_DS_RECOMA35E _FINAL6-1.pdf.
[47] H. C. de Groh, III, S. M. Geng, J. M. Niedra, R. R. Hofer, "Magnetic properties of Fe-49Co-2V alloy and pure Fe at room and elevated temperatures," NASA Glenn Res. Center, Cleveland, OH, USA, Tech. Rep. TM—2018-219872, Apr. 2018.
[48] G. Jungmayr, J. Loeffler, B. Winter, F. Jeske and W. Amrhein, "Magnetic Gear: Radial Force, Cogging Torque, Skewing, and Optimization," *IEEE Trans. Ind. Appl.*, vol. 52, no. 5, pp. 3822-3830, Sept.-Oct. 2016.
[49] S. Gerber and R-J. Wang, "Analysis of the end-effects in magnetic gears and magnetically geared machines," in *Proc. IEEE Int. Conf. Elect. Mach.*, 2014, pp. 396–402.

VIII. BIOGRAPHIES

Matthew C. Gardner (S' 15, M' 19) earned his B.S. in electrical engineering from Baylor University, Waco, Texas in 2014. He earned his Ph.D. in electrical engineering from Texas A&M University, College Station, Texas in 2019. In August 2020, he joined the University of Texas at Dallas, where he is an assistant professor. His research interests include optimal design and control of electric machines and magnetic gears.

Bryton Praslicka (S' 20) earned his B.S. in electrical engineering from Texas A&M University, College Station, Texas in 2019. He is currently pursuing a Ph.D. in electrical engineering while working in the Advanced Electric Machines and Power Electronics Laboratory at Texas A&M University. His research interests include the optimal design and control of electric machines, magnetic gears, and magnetically geared machines.

Matthew Johnson (S' 13, M'17) earned his B.S. and Ph.D. both in electrical engineering from Texas A&M University, College Station, Texas, in 2011 and 2017, respectively. He is currently an electronics engineer for the U.S. Army Research Laboratory. His research interests include the design and control of electric machines and magnetic gears.

Hamid A. Toliyat (S'87, M'91, SM'96, F'08) received the B.S, degree from Sharif University of Technology, Tehran, Iran in 1982, the M.S. degree from West Virginia University, Morgantown, WV in 1986, and the Ph.D. degree from University of Wisconsin-Madison, Madison, WI in 1991, all in electrical engineering. In March 1994 he joined the Department of Electrical and Computer Engineering, Texas A&M University where he is currently the Raytheon endowed professor of electrical engineering. Dr. Toliyat has many papers and awards to his name, including the Nikola Tesla Field Award.